Physics – Uspekhi **61** (12) 1213 – 1226 (2018)

FROM THE CURRENT LITERATURE

PACS numbers: **52.70. – m**, 52.80.Hc

Corona discharge and electrogasdynamic flows in the air

Yu K Stishkov, A V Samusenko, I A Ashikhmin

DOI: https://doi.org/10.3367/UFNe.2018.06.038358

Contents

Abstract. A corona discharge is closely related to the electrogasdynamic flows (electric wind) accompanying it. These phenomena have been considered in numerous studies and described in several monographs. Usually, they are investigated separately, because it is assumed that electric wind develops exclusively in the external region of the corona discharge. However, because a distinct boundary between the ionization layer and the external region is absent, the relation between these processes is being investigated in a number of current studies treating these phenomena in conjunction with each other. The results presented in this paper were mainly obtained in such studies.

Keywords: corona discharge, electrogasdynamics, electric wind

1. Introduction

A corona discharge (CD) is a self-sustained gas discharge in an inhomogeneous electric field [1]. Note also that is observed when several ionization collision lengths or more are fit into the gas discharge gap. Among the huge number of studies devoted to corona discharges, monographs [2, 3] should be distinguished.

A corona discharge typically consists of two regions with different properties. Ionization processes transpire in a small volume of the CD cover (in [3], the term 'ionization layer' is used) where the electric field strength is quite high. The greater part of the discharge is occupied by the so-called external region (the drift region). The electric field strength here is not high enough to produce ionization, and therefore no multiplication of charged particles occurs and they simply drift along the electric field force lines. If the polarity of a corona electrode is positive, positive ions move in the external region; if the polarity is negative, electrons and negative ions move in this region. In electronegative gases (including air), so-called attachment (the electron attachment to a molecule with the formation of a negative ion) occurs. As a result, the electron concentration rapidly decreases with distance from the corona cover. The boundary between the corona cover and external region can be determined by observing emission. In some papers, the boundary of the CD emission region is treated as the external boundary of the ionization region (corona cover).

The picture described above is observed in classical systems such as a sphere–plane, a needle–plane, and a cylinder-in-cylinder, where the characteristic radius of curvature of one of the electrodes is considerably smaller that the radius of curvature of another electrode. In this case, the first electrode is called a *corona* or *active electrode* and the second one is called a *counter electrode*. A corona discharge can also be observed in systems where the characteristic radiuses of curvature of electrodes are comparable. In this case, sheaths appear around both electrodes, and both positively and negatively charged particles move in the drift region. Such a corona is called bipolar and is not considered in this review.

A corona discharge is characterized by strong negative feedback between a volume discharge in the external region and the electric field in the cover. Because the charge polarity in the external region coincides with the polarity of the corona electrode, the field of this charge tends to reduce the electric field strength in the cover. The decrease in the field strength slows down ionization in the cover and reduces the current from the cover to the external region. Due to such an interrelation, the electric field strength in the cover barely changes with increasing voltage. This circumstance is used in various approximate CD calculation methods, for example, the Deich–Popkov method [3].

Corona discharges with positive and negative polarities are two substantially different phenomena. Differences between negative and positive coronas are shown schematically in Fig. 1. A corona discharge belongs to the class of self-sustained phenomena proceeding without the continuous

Yu K Stishkov, A V Samusenko, I A Ashikhmin
Saint Petersburg State University,
Universitetskaya nab. 7-9, 199034 St. Petersburg, Russian Federation
E-mail: y.stishkov@spbu.ru, andreys2004@yandex.ru

Received 4 August 2017, revised 24 April 2018
Uspekhi Fizicheskikh Nauk **188** (12) 1331 – 1345 (2018)
DOI: https://doi.org/10.3367/UFNr.2018.06.038358
Translated by M N Sapozhnikov

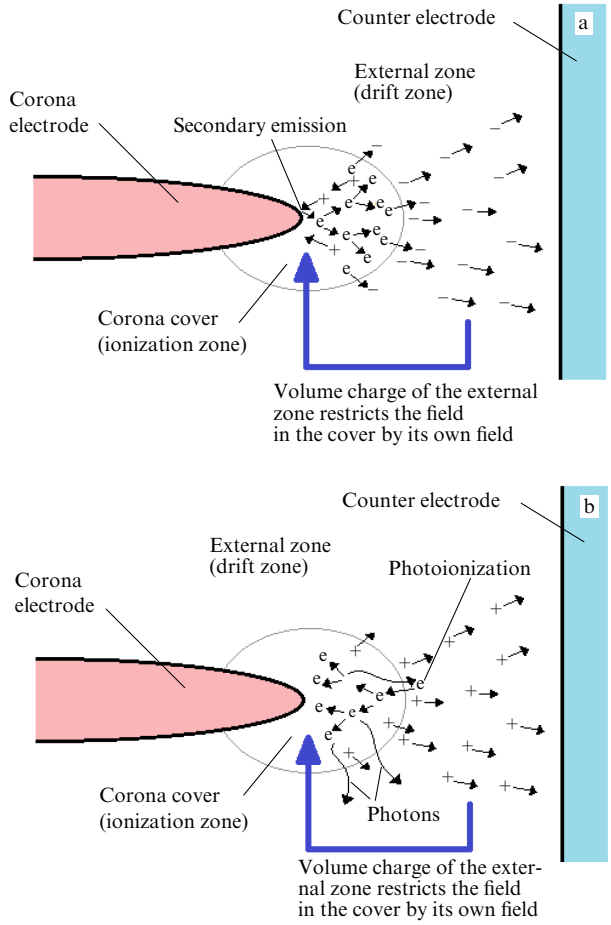

Figure 1. Structures of negative (a) and positive (b) corona discharges.

action of any external ionization source. The reproduction of electrons in the case of negative polarity is provided by secondary ion–electron emission, when positive ions incident on the cathode surface knock out electrons with the probability γ, thereby initiating the next avalanche. The dimensionless coefficient γ is called the secondary emission coefficient.

In the case of a positive CD, secondary electrons are produced due to photoionization caused by photons escaping from the CD sheath. These features determine the considerable structural varieties of the CD sheath. In the case of a negative CD, electrons appear on the electrode surface and fly from it, ionizing surrounding gas molecules. Because of this, the maximum ionization region is located at some distance from the electrode surface. This distance is of the order of ten mean free paths. Then, ionization decreases due to a decrease in the electric field strength.

In a positive CD, electrons appear at some distance from the electrode surface and fly from it, producing ionization. Therefore, the maximum ionization region is adjacent to the electrode surface.

The literature on the gas discharge physics can be found in [4].

In [5], transitions among corona, glow, and spark discharges caused by nanosecond voltage pulses are considered. Similar transitions in the case of a constant voltage are considered in [6].

The appearance of a corona discharge initiates the motion of air, because the moment imparted by the Coulomb force to charged particles in elastic collisions is efficiently distributed over neutral molecules. A flow appears, which was called the 'electric wind' (EW) [3]. As a rule, this is a thin intense jet directed from a high-voltage electrode to a grounded electrode.

Effects related to the electric wind play a considerable role in industrial electric filters [3]. Possible EW applications for cooling solid surfaces [7–11] and building aircraft [12, 13] are under study. Experiments have shown that the EW changes the streamline profile of various bodies. Thus, the influence of a corona discharge on a stream flowing around a plate in a wire–plane electrode system was demonstrated in [14] by the method of particle image velocimetry. The possibility of CD controlling a flow over a flat plate was studied subsequently in [15]. A computer simulation of the EW in the unipolar approximation for studying CD influence on the air flowing around various bodies was performed in [2, 16–19]. The EW role in a system for water purification from organic contaminants was analyzed in [20]. It was shown that ozone produced in the CD sheath penetrates into water considerably faster under the influence of the EW, which increases the rate of water purification from contaminants. A constant-voltage CD was used in [21] for air purification from toluene. The authors have managed to achieve a purification efficiency of up to 93%.

In [22], a multielectrode system is presented in which the airflow caused by a corona discharge is used for rapid drying.

The calculation of the electric wind requires a description of the air aerodynamics and discharge processes. These processes have substantially different spatial and time scales, and therefore the numerical calculation of the EW problem requires a long time and a large memory volume. Thus, the construction of simplified EW models is urgent.

In [23], a barrier discharge from a blade electrode located on a solid dielectric substrate is simulated in a plane-symmetrical system. The simulation was performed in the drift-diffusion approximation. The calculated distribution of the volume Coulomb force was comparable with the analytic estimate. Gas flows (electric wind) were not calculated in [23], and any comparison with experiments is absent. In [24], it was reported that CD processing considerably changes the properties of polypropylene and polyethylene surfaces.

The use of discharges of several types, including corona discharges, to stabilize a flame is considered in [25]. The efficiency of this method depends on the electrode location. The emission spectrum of the flame depends on the electrode location and the discharge type.

Considerable attention is given in the literature to plasmochemical reactions in a CD and the use of a corona as a source of active materials applied to process, purify, and disinfec surfaces. In [26], the characteristics of a CD ozon generator are presented. Reactions related to the interaction of CD products with water are considered in [27]. The process of removing phenol from water with the help of a CD was studied in [28].

The composition of negative ions in the external region of a negative CD was analyzed with a mass spectrometer in [29]. It was found that the composition strongly changed due to reactions with O_3 and NO_2 produced in the corona cover. These reactions lead to transformations of negative ions to NO_3^- and $NO_3^-HNO_3$. These ions are called terminal ions in [29].

The reactive force of an EW jet can be used as a lifting force for building an aircraft. However, because of the low

efficiency, such aircraft still require an external electric energy supply with the help of wires [13].

Numerous recent studies in gas discharge physics were performed using the Cosmol Multiphysics software package, allowing numerical calculations of basic systems of partial differential equations involved in this field of physics [30–33].

2. Corona discharge shapes

Let us consider and analyze some results of CD studies [34].

Differences in CD shapes for negative and positive polarities are not considered in detail, as a rule. However, modern experimental CD studies with sensitive cameras allow one to find these differences [34]. Figure 2 shows the video frames of a CD cover near the surface of a sphere electrode for the negative and positive polarity of this electrode. The photographs demonstrate distinct differences in the emission regions of the positive and negative coronas. In the case of the negative potential of a corona electrode, the focus CD shape is observed in most electrode systems. Figure 2 shows photographs of a light region (we will call it the CD cover) near the surface of a wire electrode in the cylinder-in-cylinder (b) and sphere–plane (a) systems.

It can be seen that the homogeneous surface of a sphere electrode contains a distinct CD focus. The emission structure of an individual focus is approximately axially symmetric and resembles a mushroom in cross section: there is a small active spot on the pole of a sphere electrode from which a short cylindrical emitting region (stem) and a conical expanding part with a diffusion external boundary (cap) grow. Similar focuses with less regular shapes are observed on the surface of a cylindrical electrode (Fig. 2b). As the sphere electrode diameter is increased, the number of focuses increases.

A corona discharge from a positive electrode has a considerably different structure. The shape and character of a positive CD substantially depend on the shape and size of the corona electrode and the homogeneity of the electrode surface. Any surface inhomogeneity gives rise to a streamer CD. In the case of a sphere electrode with a polished homogeneous surface, the sheath of a positive CD has the form of a thin luminous layer around the sphere electrode surface (Fig. 2a). The luminous spherical layer repeats the electrode shape and has a thickness of about 0.1 mm, the emission brightness being higher near the lower pole of the sphere, decreasing the upper pole of the sphere, which correlates with the field strength distribution over the sphere surface. A similar shape can be observed on a thin cylindrical electrode (Fig. 2b). Here, a thin continuous luminous layer is also observed near the cylindrical electrode surface. The focus structure is completely absent. Thus, simulations of the CD sheath should take into account the corona electrode polarity.

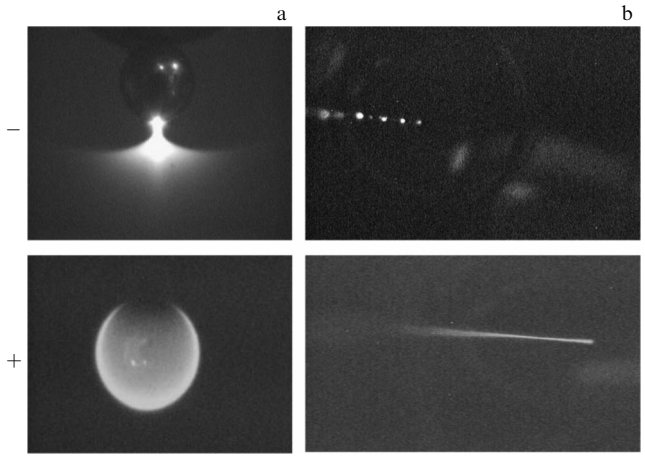

Figure 2. Photographs of a CD cover near the spherical electrode surface (a) and wire (b) for negative (−) and positive (+) polarities. (a−) sphere diameter is 0.7 mm, interelectrode distance is 20 mm, voltage is 26 kV; (a+) sphere diameter is 2 mm, interelectrode distance is 20 mm, voltage is 24 kV; (b) corona wire diameter is 0.09 mm, grounded cylinder diameter is 33 mm.

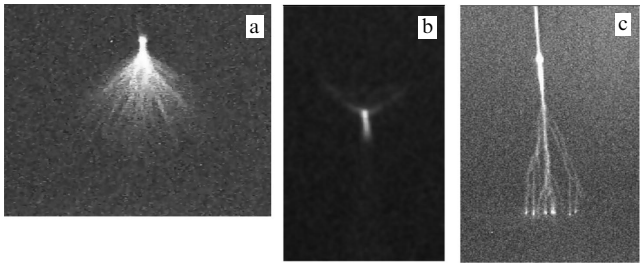

Figure 3. Streamer shape of a positive CD. The needle rounding radius is 0.1 mm. (a) Primary streamer form, needle electrode, 10 kV, interelectrode distance is 10 mm. (b) Degenerate primary streamer form, needle electrode, magnified scale — needle point photo, 9 kV, interelectrode distance is 10 mm. (c) Developed streamer form, needle electrode, 20 kV, interelectrode distance is 20 mm.

In the case of a rough surface or a needle electrode and positive polarity, a corona discharge has a streamer shape in a broad voltage range. In this case, in some range beginning from the threshold voltage, relatively short streamers are observed (Fig. 3a) which sometimes degenerate into a single nonbranching short channel (Fig. 3b; this shape can be called the 'primary streamer' shape). Then, the voltage range follows where the surrounding corona described above is observed. As the voltage is further increased, streamers appear again (Fig. 3c); their length is comparable to or reaches the interelectrode gap value.

3. System of equations for a corona discharge in the drift-diffusion approximation

Consider a system of equations describing a corona discharge in air. In the drift-diffusion approximation, this system contains three Nernst–Planck equations for electrons, negative and positive ions, and the Poisson equation [35]

$$\begin{aligned}
&\frac{\partial n_e}{\partial t} + \operatorname{div}\left[-D_e \nabla n_e - n_e \mu_e \mathbf{E}\right] = \alpha_0 \mu_e E \exp\left(-\frac{E_0}{E}\right) n_e - \nu_{att} n_e\,,\\
&\frac{\partial n_+}{\partial t} + \operatorname{div}\left[-D_+ \nabla n_+ + n_+ \mu_+ \mathbf{E}\right] = \alpha_0 \mu_e E \exp\left(-\frac{E_0}{E}\right) n_e\,,\\
&\frac{\partial n_-}{\partial t} + \operatorname{div}\left[-D_- \nabla n_- - n_- \mu_- \mathbf{E}\right] = +\nu_{att} n_e\,,\\
&\varepsilon_0 \Delta\varphi = -e(n_+ - n_e - n_-)\,, \quad \mathbf{E} = -\nabla\varphi\,.
\end{aligned} \tag{1}$$

The required functions are the concentrations of electrons, negative and positive ions n_e, n_-, and n_+, respectively, and the electric potential φ. The ionization and attachment rates are assumed to be known.

Using the ratio D_e/μ_e as the potential unit, which is approximately equal to the mean electron energy in electron volts, we obtain the dimensionless potential $\Phi = \varphi\mu_e/D_e$. The

characteristic length unit can be constructed in the form $e\mu_e/D_e\varepsilon_0$. This gives the characteristic concentration unit $(e\mu_e/D_e\varepsilon_0)^{-3}$. The characteristic time unit can be written in the form $(e\mu_e/D_e\varepsilon_0)^2/D_e = (e\mu_e/\varepsilon_0)^2/D_e^3$. Using these measurement units, we obtain a system of equations in the dimensionless form:

$$\frac{\partial N_e}{\partial T} + \mathrm{div}'\,[-\nabla' N_e - N_e \boldsymbol{\Sigma}] = \frac{\psi_{ion}}{\lambda_{ion}} \exp\left(-\frac{\psi_{ion}}{\Sigma}\right) N_e - Y_{att} N_e\,,$$

$$\frac{\partial N_+}{\partial T} + \mathrm{div}'\,[-\delta_+ \nabla' N_+ + N_+ m_+ \boldsymbol{\Sigma}] = \frac{\psi_{ion}}{\lambda_{ion}} \exp\left(-\frac{\psi_{ion}}{\Sigma}\right) N_e\,,$$

$$\frac{\partial N_-}{\partial T} + \mathrm{div}'\,[-\delta_- \nabla' N_- - N_- m_- \boldsymbol{\Sigma}] = +Y_{att} N_e\,,$$

$$\Delta' \Phi = -(N_+ - N_e - N_-)\,, \quad \boldsymbol{\Sigma} = -\nabla' \Phi\,.$$

This system of equations contains dimensionless parameters: dimensionless diffusion coefficients $\delta_- = D_-/D_e$ and $\delta_+ = D_+/D_e$ and dimensionless mobilities $m_- = \mu_-/\mu_e$ and $m_+ = \mu_+/\mu_e$. The source function contains the dimensionless ionization length $\lambda_{ion} = \varepsilon_0 D_e/\alpha_0 e\mu_e$, the dimensionless ionization energy $\psi_{ion} = e\mu_e^2 E_0/\varepsilon_0 D_e^2$, the dimensionless attachment rate $Y_{att} = \nu_{att}/D_e^3(e\mu_e/\varepsilon_0)^2$, and the dimensionless voltage $U\mu_e/D_e$. Also, dimensionless geometrical parameters are used. For example, two dimensionless parameters in a sphere–plane system are the electrode radius $R\varepsilon_0 D_e/e\mu_e$ and the interelectrode distance $h\varepsilon_0 D_e/e\mu_e$.

4. Computer models of negative and positive corona discharges

Computer simulations of a CD have been performed in many studies. They differ in the formulation of the problem and in the means applied. Consider the results of a simulation of a negative CD obtained using the Comsol Multiphysics software package. In [35], the structure of the sheath of a negative CD was analyzed in detail and the physical mechanism of formation of the focus form in a negative CD was first explained. Simulations of a positive CD were performed in [36].

The calculation of a positive CD should take into account photoionization. This model uses the simplified equation considered in detail in [37]. The photon concentration n_{ph} is described by the equation

$$-\Delta n_{ph} = -\lambda^2 n_{ph} + \frac{\lambda}{c} q_{ph}\,.$$

Here, q_{ph} is the source of photon creation in electron impacts, and λ is the absorption coefficient for ionizing radiation (in m^{-1}). Its dependence on the field strength is specified similarly to the dependence of the ionization coefficient on the field strength, because the transition energies for these two processes are close (since ionizing photons are emitted from the highest energy levels of a molecule):

$$q_{ph} = g\nu_{ion}(E) n_e\,. \qquad (2)$$

Here, g is the dimensionless ionization efficiency, ν_{ion} is the electron-impact ionization rate, n_e is the electron concentration, and E is the field strength.

For electrons, a source related to photoionization is added:

$$\frac{\partial n_e}{\partial t} + \mathrm{div}\,[-D_e \nabla n_e - n_e \mu_e \mathbf{E}] = \ldots + \lambda c n_{ph}\,. \qquad (3)$$

Thus, the system of equations

$$\frac{\partial n_e}{\partial t} + \mathrm{div}\,[-D_e \nabla n_e - n_e \mu_e \mathbf{E}] = \alpha_0 \mu_e E \exp\left(-\frac{E_0}{E}\right) n_e - \nu_{att} n_e + \lambda c n_{ph}\,,$$

$$\frac{\partial n_+}{\partial t} + \mathrm{div}\,[-D_+ \nabla n_+ + n_+ \mu_+ \mathbf{E}] = \alpha_0 \mu_e E \exp\left(-\frac{E_0}{E}\right) n_e + \lambda c n_{ph}\,,$$

$$\frac{\partial n_-}{\partial t} + \mathrm{div}\,[-D_- \nabla n_- - n_- \mu_- \mathbf{E}] = +\nu_{att} n_e\,,$$

$$-\Delta n_{ph} = -\lambda^2 n_{ph} + \frac{\lambda}{c} g\alpha_0 \mu_e E \exp\left(-\frac{E_0}{E}\right) n_e\,,$$

$$\varepsilon_0 \Delta\varphi = -e(n_+ - n_e - n_-)\,, \quad \mathbf{E} = -\nabla\varphi \qquad (4)$$

is solved for both positive and negative polarities.

System (4) is supplemented by hydrodynamic equations. The air motion appears due to momentum transfer from charged particles to surrounding neutral molecules in elastic collisions. As a result, we can assume that the Coulomb force acting on charged particles is directly applied to air as a whole:

$$\rho \frac{\partial \mathbf{v}}{\partial t} + \rho(\mathbf{v}\nabla)\mathbf{v} = -\nabla P + \eta\Delta\mathbf{v} + e(n_+ - n_e - n_-)\mathbf{E}\,, \qquad (5)$$

$$\mathrm{div}\,\mathbf{v} = 0\,.$$

The CD properties are determined by the electric-field direction and, therefore, by the direction of flight of ionizing electrons.

As in experiments, computer models consider the sphere–plane electrode system (Fig. 4). Boundary conditions are presented in Table 1.

We used coefficients $\mu_+ = \mu_- = 2{,}8 \times 10^{-4}$ m^2 V^{-1} s^{-1} and the secondary emission coefficient $\gamma = 3 \times 10^{-4}$ (see Table 1).

The results of simulations for positive and negative CDs and their analysis are presented below [34]. Figure 5 shows the field strength distributions along a sphere electrode surface for two voltages: before the 10-kV threshold (solid curve) and after CD ignition at 12 kV (dashed curve). Figures 5a and 5b correspond to negative and positive CDs, respectively. The

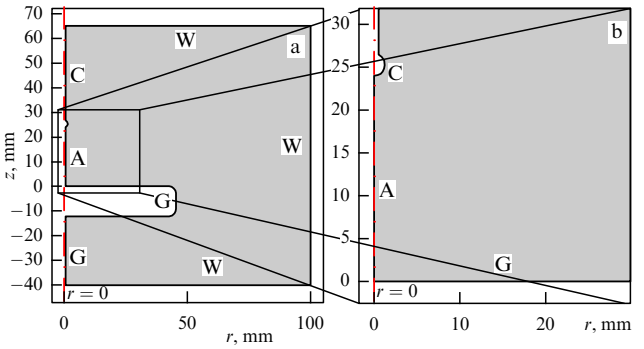

Figure 4. (a) Geometry of the corona discharge computer model. (b) Region of interest at a larger scale.

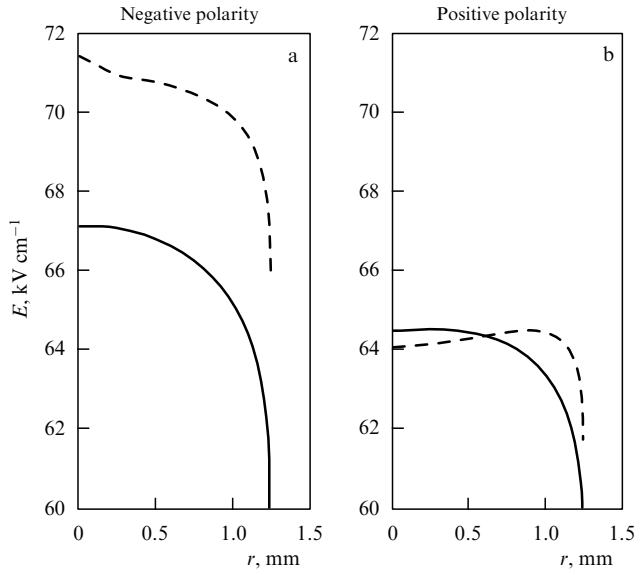

Figure 5. Field strength distributions along the spherical electrode surface. 10 kV — solid curve, 12 kV — dashed curve.

Table 1. Boundary conditions.

Negative corona				
	C	G	A	W
φ	$\varphi = -U$	$\varphi = 0$	$\partial\varphi/\partial r = 0$	$\partial\varphi/\partial n = 0$
n_e	$j_{e,n} = -\gamma j_{+,n}$	—	$j_{e,r} = 0$	$j_{e,n} = 0$
n_-	$j_{-,n} = 0$	—	$j_{-,r} = 0$	$j_{-,n} = 0$
n_+	—	$j_{+,n} = 0$	$j_{+,r} = 0$	$j_{+,n} = 0$
n_{ph}	$\partial n_{ph}/\partial n = 0$			
Positive corona				
φ	$\varphi = +U$	$\varphi = 0$	$\partial\varphi/\partial r = 0$	$\partial\varphi/\partial n = 0$
n_e	—	$j_{e,n} = 0$	$j_{e,r} = 0$	$j_{e,n} = 0$
n_-	—	$j_{-,n} = 0$	$j_{-,r} = 0$	$j_{-,n} = 0$
n_+	$j_{+,n} = 0$	—	$j_{+,r} = 0$	$j_{+,n} = 0$
n_{ph}	$\partial n_{ph}/\partial n = 0$			

field strength distribution in a CD differs from that undisturbed by a volume charge. For a negative corona, the field somewhat increases near the sphere pole — the symmetry axis (this zone becomes a corona focus–electrode contact region) — while for a positive corona, the field almost uniformly decreases over the entire surface and the field strength minimum rather than the maximum is formed at the center (see Fig. 5). The local extremum of the field strength appears due to a volume charge produced in the sheath of the negative CD. This charge also reduces the field in the sheath of the positive CD.

The ionization regions of negative and positive coronas have a corresponding look (Fig. 6). Note that the local dimensions of the effective ionization regions are substantially different for negative and positive coronas, are rather small, and do not exceed 500 μm.

Figure 6 demonstrates stationary ionization intensity distributions in the region close to the electrode end for negative (a) and positive (b) CDs. These distributions are

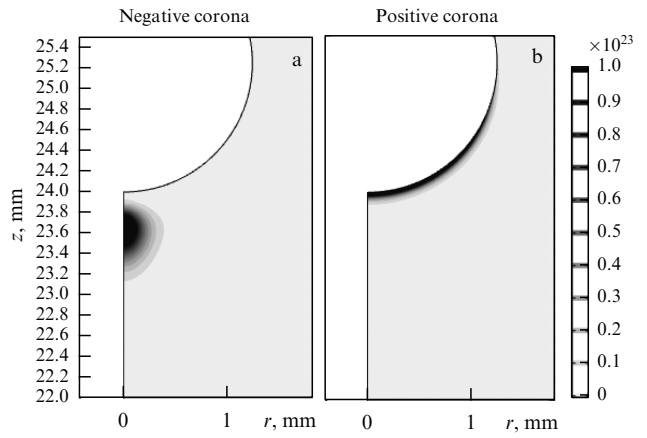

Figure 6. Ionization intensity distributions (in m^{-3} s^{-1}). (a) Negative polarity, (b) positive polarity. 5.4-μA current.

substantially different. The ionization zone for the negative CD has an egg-like shape with the local size of about 500 μm. Note that this picture is formed during the CD development, and the initial distribution of the force lines of the field is virtually uniform. The local extremum of the field strength appears because of a volume charge produced in the CD focus due to separation of positive ions and electrons and also due to secondary ion–electron emission. This leads to an increase in the concentration of charged particles in the region of increased ion–electron emission and to the enhancement of the flux of secondary electrons in a small spot on the pole of a sphere electrode. Note that the displacement of the effective ionization region is quite small and does not exceed 100 μm. The displacement is explained by the necessity of acquiring energy by secondary electrons appearing in the higher-field strength region on the sphere electrode surface. For a positive CD, the ionization zone is a thin layer near the electrode surface, the ionization maximum being adjacent to the electrode surface. This is explained by the fact that ionizing electrons in this case fly to the sphere surface.

Figure 7 presents the distributions of the field strength and concentration of charged particles near the electrode. One can see that, for the negative polarity, on moving to the self-sustained discharge regime, a CD cover focus with a transverse radius of about 500 μm is formed in the axial region where ionization processes are concentrated. Because of this, positive ions coming from the ionization region are concentrated in the axial region near the sphere surface. The concentration of electrons coming from the ionization region is also maximal in the axial region at a distance of about 100 μm from the cathode surface. The electron flux increases from the cathode surface due to impact ionization, and, further, at a distance of about 100 μm, the electron annihilation region dominates where electrons attach to oxygen molecules and the electron flux decreases. This explains the presence of the maximum of electron concentration. Outside the axial region with the transverse size of 20 μm, ionization is almost absent.

In the case of positive polarity, the distribution region of electrons has the form not of a focus but of a thin layer surrounding the electrode surface.

The presence of a narrow field-strength maximum in the case of negative polarity is related to the distribution of charged particles. The cloud of positive ions in the CD cover coming from the ionization region and concentrated near the

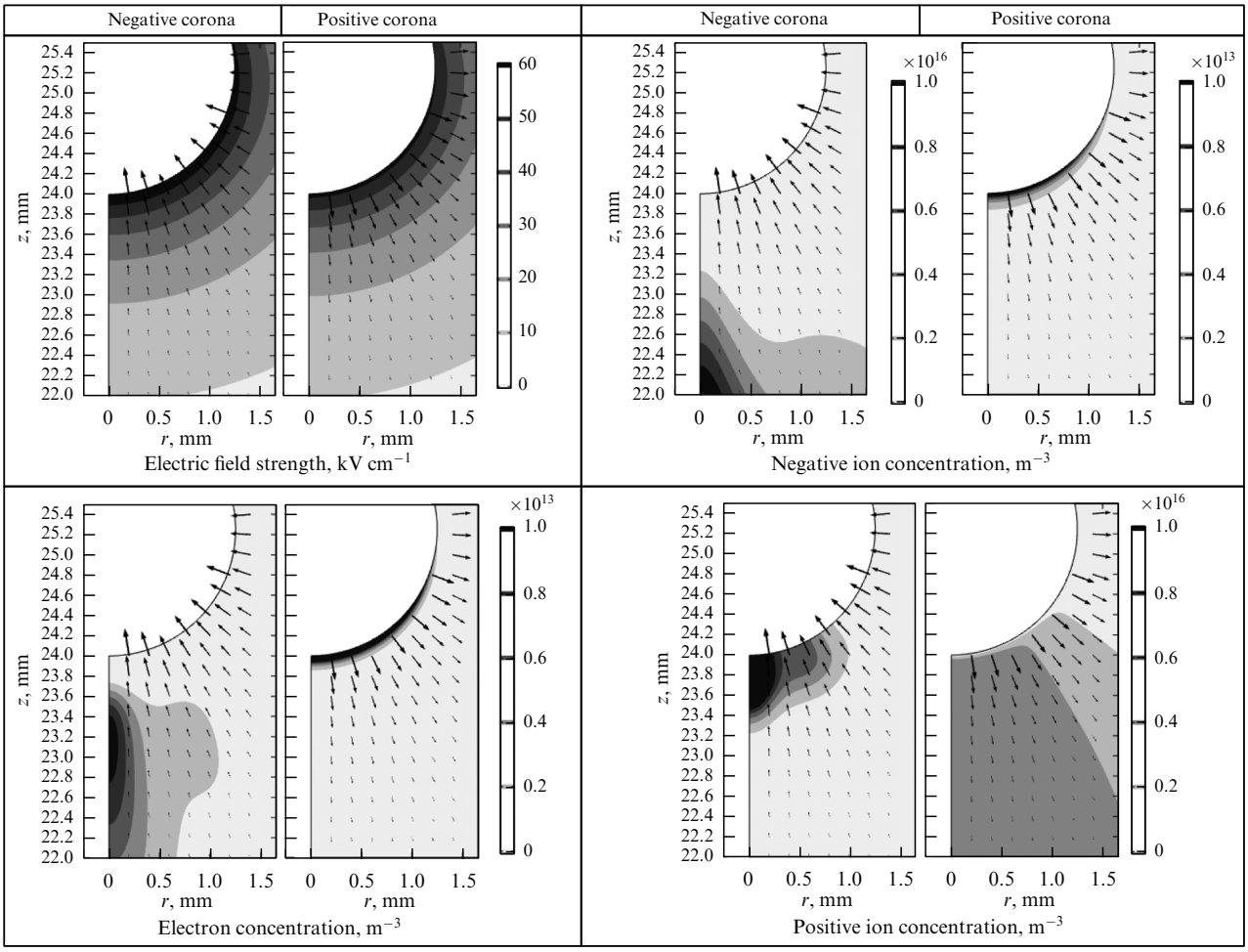

Figure 7. Electric field strength and concentration distributions for positive and negative coronas, 5.4-μA current.

symmetry axis enhances the field on the cathode pole and partially screens the action of negative ions of the external region. The charge of positive ions is considerably smaller than that of negative ions; however, their influence is noticeable near the CD cover. The separated charge structure in the corona cover causes a tightening of the force lines of the field and forms a separated focus, preventing the cover's 'spreading' over the needle. As a result, in the developed CD regime, unlike the threshold stage of a self-sustained discharge, an enhanced-ionization local region is formed near the axis (see Fig. 5), which determines the transverse boundaries of the CD focus. Because of the attachment of electrons to oxygen molecules, a flux of negative ions appears from the focus region, migrates along the force lines of the field, and escapes, diverging from the CD cover and forming a peculiar mushroom-like luminous cap. For a positive CD, the picture is different. In this case, no negative ions appear, electrons rapidly disappear on the electrode, and positive ions produced in a thin layer near the sphere electrode surface slightly reduce the field near its surface. In this case, focuses do not appear.

The model does not use the artificial separation of the cover and external region, because one system of equations (4), (5) is solved for the entire interval. We can assume that the formal boundary of the cover is a zone where the electron creation rate of impact ionization exceeds the electron annihilation rate due to the attachment of electrons to oxygen molecules. This zone on the symmetry axis does not exceed 1000 μm from the cathode, irrespective of voltage. Note, however, that the emission region is considerably broader [38]. This is explained by the fact that the CD emission appears first of all due to excitation of gas molecules in collisions with electrons. These reactions have lower energy thresholds than impact ionization and, therefore, the efficient emission can be observed at a lower field strength than in the case of ionization. For this reason, the emission region in a CD always occupies a greater volume than the ionization region. Note that the force lines of the electric field are strongly distorted by a volume discharge, as shown in Fig. 8: while in the state undisturbed by a volume discharge, the force lines radially diverge from the hemispherical surface of the 'needle' end; in the developed CD regime, the force lines are tightened to the symmetry axis in the localization region of a positive microcloud and then diverge. Because the migration current caused by the electric field dominates over the diffusion current in the system, the electron transfer occurs almost along the force lines of the electric field. The distortion of lines provides the specific mushroom-like shape of the CD focus observed in experiments (see Fig. 2): a thin 'stem' near the negative needle electrode and a broad diffusion 'cap'.

Outside the cover of a negative CD, positive ions are absent, the electron concentration is low, and the charge transfer is provided by negative ions. The concentration of

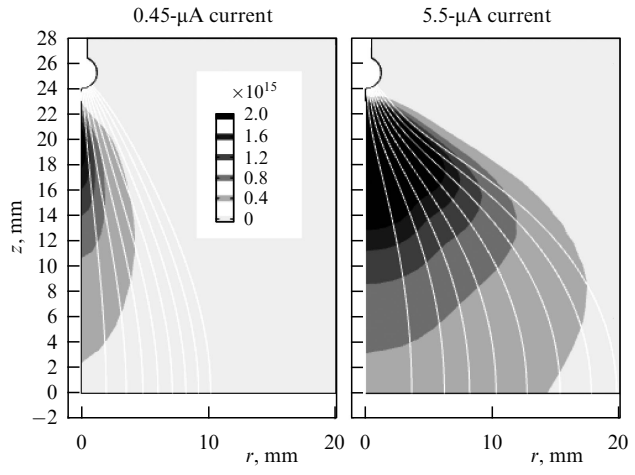

Figure 8. Negative ion concentrations and force lines of an electric field for different corona currents. Negative corona.

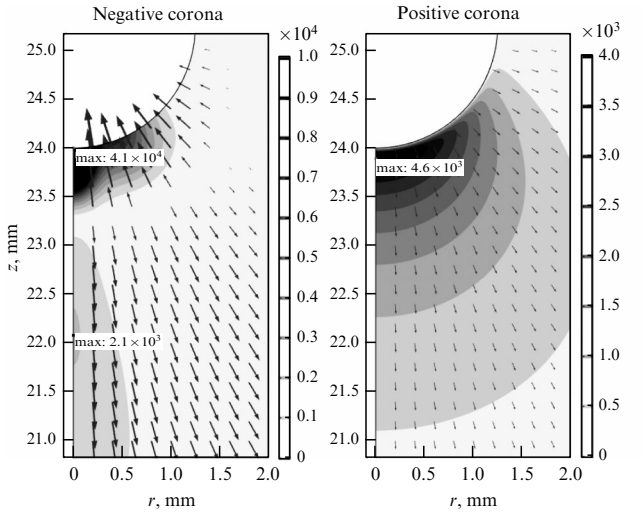

Figure 9. Distributions of the volume Coulomb force (in C m^{-3}). 5.4-μA current.

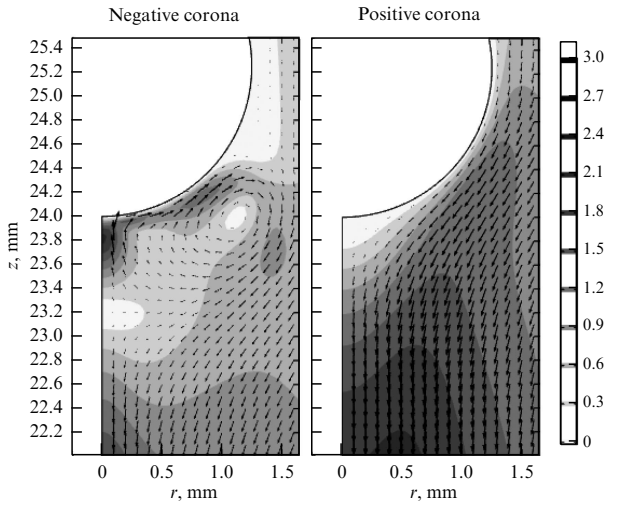

Figure 10. Distributions of air velocity (in m s^{-1}) near the electrode. 5.4-μA current.

negative ions and force lines of the electric field in the external CD region are shown in Fig. 8. The force lines in the external region are also distorted by a volume discharge. Because the charge of ions is negative, the force lines bend round it, and the cloud of negative ions is sort of pushed apart under the action of the Coulomb force. Thus, the statement that the ionization region is uniformly distributed over the surface of an injecting electrode is incorrect for a negative CD. The ionization region is concentrated on the injecting electrode end and, although the ionization region size remains invariable, electric-field distributions in the external region considerably change with increasing voltage, the divergence of force lines increases, and the size of the region to which ions on a counter electrode come increases.

Thus, models for positive and negative polarities are substantially different, the results of simulations corresponding to experimental data. In the case of positive polarity, electrons are distributed by a thin layer over the surface of a spherical electrode, while in the case of negative polarity, electrons form a cloud elongated along the symmetry axis. Thus, the model reproduces the focus shape of a negative corona and the surrounding shape of a positive corona.

The shape of the electron distribution also determines the ion distribution in the external region: the distribution of negative ions in the negative corona takes a mushroom-like shape, with a thin stem expanding with distance from the sphere. On the contrary, positive ions in the positive corona diverge from the sphere in the form of a broad flux from the entire surface of the spherical electrode. Note also that in the case of a negative corona, electrons depart comparatively far away from the sphere surface. As a result, the cloud of negative ions is separated from the sphere by approximately a 1-mm gap. By contrast, this gap in the positive corona is extremely small, less than 0.1 mm.

The focus shape determines the distribution of the Coulomb force moving air (Fig. 9). In the case of a negative corona, there are a small compact ionization region with a powerful force directed from the ionization region to the spherical electrode and a broader region with a force directed from the ionization region to the counter electrode. In the case of a positive corona, the Coulomb force is directed from the spherical electrode and is distributed along its surface.

Differences also exist in the structure of the appearing electric wind. In the case of negative polarity, differently directed forces produce a microscopic vortex near the surface of the spherical electrode, whereas a vortex is absent in the case of positive polarity (Fig. 10). The microvortex causes instability of the CD focus with respect to the electrode surface. Small fluctuations of the CD cover with respect to the symmetry axis are observed in experiments.

On a large scale, flows for different polarities are quite similar (Fig. 11). Note that, although the field directions are opposite, the flows are determined by the motion of ions. Because of this, the main stream is directed in both cases from the sphere to the plane. In the case of positive polarity, the stream is somewhat broader. This is related to the greater radial size of the Coulomb force region for the positive polarity than the narrow focus for negative polarity. However, in systems with a different geometry, where the focus size exceeds the rounding radius of the electrode, a different situation is possible; in particular, in a needle–plane system, the electric wind stream for the

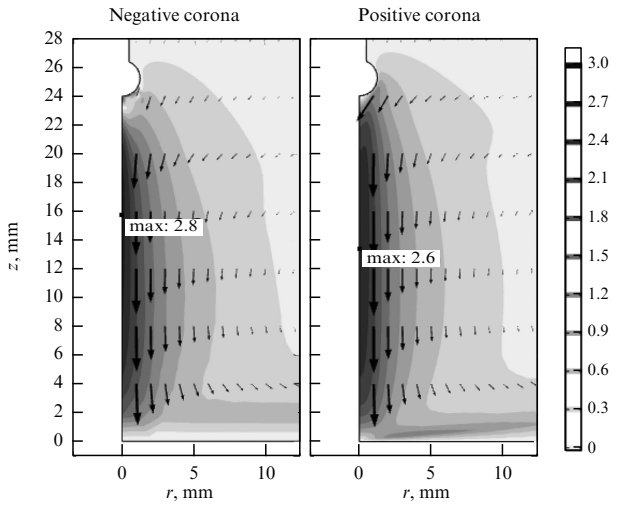

Figure 11. Distributions of air velocities (in m s^{-1}). 5.4-μA current.

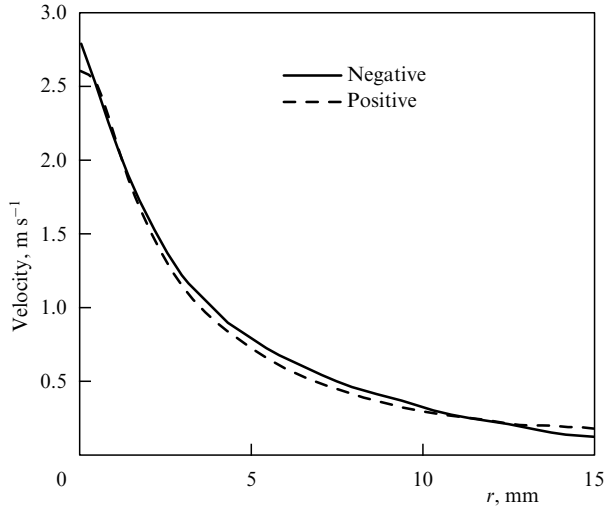

Figure 12. Distribution of the axial velocity component on a line drawn in the middle of the interelectrode gap. 5.4-μA current.

positive corona is considerably narrower than that for the negative one.

Figure 12 presents EW velocity profiles for positive and negative coronas in the middle of the interelectrode gap. One can see that they coincide in fact.

5. Experimental laser anemometry study of the electric-wind kinematic structure

It is known that a CD combustion in air is accompanied not only by ionization processes but also by the motion of a neutral medium in the interelectrode gap, which is called electric wind. This phenomenon found applications in various technologies and devices, for example, electric filters, electrohydrodynamic actuators, ionic engines, and heat-exchange intensification devices [3].

The experimental study of EW kinematics is a quite complicated question [39, 40], because the CD combustion results in the formation of a spatial charge and is possible only in the region of high electric fields. For this reason, so far it has been possible to measure EW velocities only outside the CD cover. In this section, we present the results of measuring the velocity field in a needle–torus system for various polarities of the applied voltage on a modern La Vision FlowMaster setup.

The EW kinematics were studied in a needle–torus electrode system. This system is convenient because the EW jet freely propagates through a hole in a counter electrode, not producing return vortices. The velocity field was studied by the method of particle image velocimetry (PIV) in the completely automatic mode. The velocity field was measured with a La Vision FlowMaster setup at the Geomodel resource center, St. Petersburg State University. The method is based on a statistical analysis of the most probable displacement of an ensemble of particles. Images were recorded by the PIV method in the following way. A laser beam was focused with a cylindrical lens, similarly to an optical knife on a certain plane in a cell. The width of the optical knife was estimated at 0.5–1.0 mm. The image obtained was fixed with an ImageproX TV camera with an intensity resolution of 14 bits and a 1200×1600 array and was then processed using DaVis software. The PIV method involves the recording of two successive frames separated by a fixed time interval. The time between laser shots was chosen so that the displacement between visualizing particles was greater than one pixel and smaller than one fourth of the search window size.

One of the important aspects of the PIV study of EW is the choice of particles for visualization. French researchers [41] compared various materials for visualizing flows in air, such as cigarette smoke, oil, and SiO_2 and TiO_2 microspheres. They showed that visualization with the help of oil and SiO_2 microspheres cannot be used in EW studies, because these materials change the current in the system by an order of magnitude.

The authors of [41] also proposed dimensionless criteria such as the Stokes number, the Archimedes number, and the mobility relation. They showed that particles smaller than 1 μm satisfy these relations and, therefore, can be used for visualization. The visualization was performed using the dioctyl ether of sebacic acid (DEHS). This substance was also used in [42]. DEHS was sprayed with an aerosol generator supplied together with the setup. The mean diameter of individual particles specified by the manufacturer was 500 nm, while the generation rate was approximately 100 million units per second.

In experiments, a linearly increasing voltage is applied to a system of electrodes, and a corona is ignited above a threshold voltage. The corona ignition is necessary for the appearance of the electric wind, and after its appearance, the entire medium begins to move, including visualizing particles.

Consider the EW velocity fields in air in a needle–torus electrode system obtained for different polarities when the voltage linearly increases from the ignition threshold up to 15 kV.

The negative polarity offers a greater variety of observed phenomena. It is known that, at the corona ignition threshold in the case of negative polarity, the corona has a blinking character and the current flowing in the system is pulsed (so-called Tritchel pulses, whose repetition rate rapidly increases with increasing voltage), and the corona begins to burn stably at high voltages. In experiments below the corona ignition threshold, a current was observed whose value was a few orders of magnitude lower than the current flowing during the corona combustion.

As already mentioned, when the voltage in the system was further increased, Tritchel current pulses were detected at the

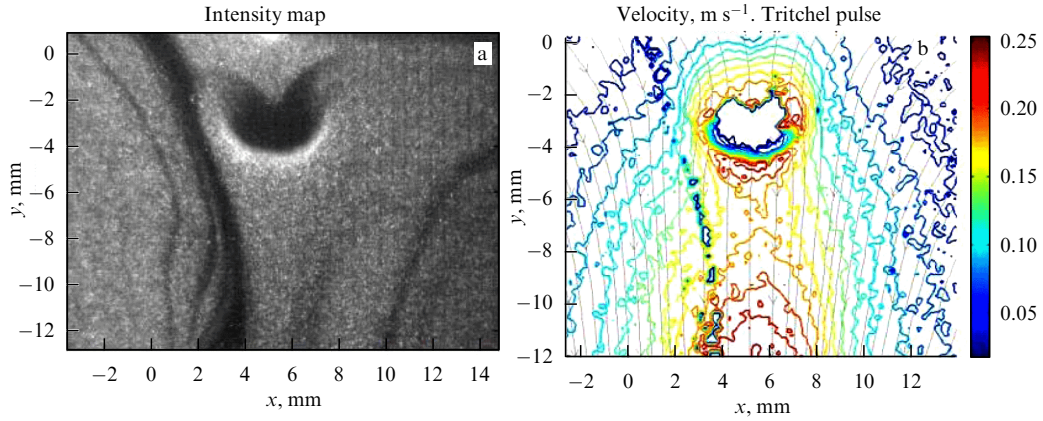

Figure 13. Distributions of visualized particles (a) and velocity (b) in the phase of Tritchel pulses of the negative corona discharge.

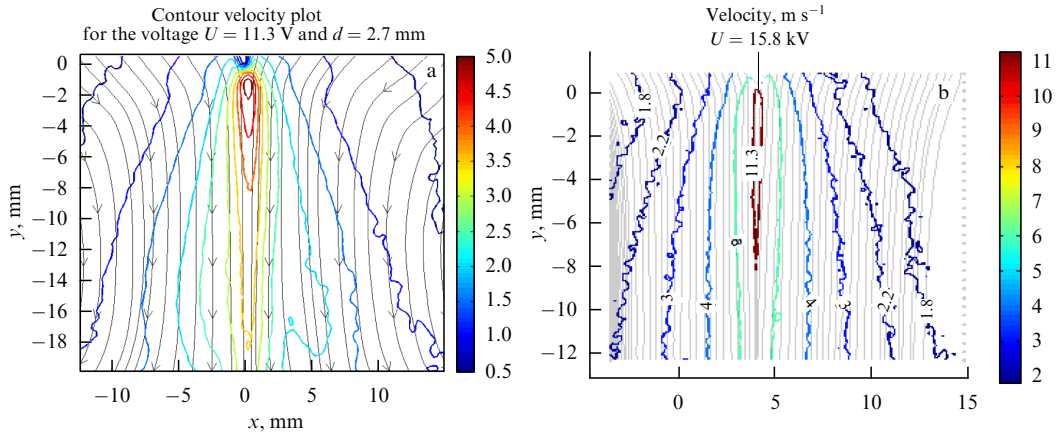

Figure 14. EW current lines and EW velocity level lines; (a) negative and (b) positive needle polarities.

corona ignition threshold, their repetition rate increasing with increasing voltage. The nature of Tritchel pulses is related to the strong influence of a volume charge on the secondary ion–electron emission from the surface of a needle electrode. For a voltage close to the threshold, the pulse repetition rate is lower than 1 Hz. In this case, a video camera gives the following picture: at the moment of corona ignition, an air region, which does not, in fact, contain visualizing particles, appears from the needle electrode and moves to the volume. Figure 13 shows the typical distribution of visualizing particles near the needle electrode.

Light points correspond to individual visualized particles. We see the bright region at the top (coordinates x — 6 mm and y — 0) corresponding to reflection from the needle. Under the needle, a mushroom-like region without visualized particles is located. This region appears in the negative corona cover with the same mushroom-like shape simultaneously with the cover ignition, i.e., simultaneously with a single current pulse, and possibly contains the volume charge at the higher concentration, because it moves under the action of the electric field from top to bottom with a velocity of about 30 cm s^{-1} (see Fig. 13).

As the voltage was increased, the current pulse repetition rate increased, and simultaneously the number of such regions in the camera field of view increased linearly with voltage. The regions are located along the flow axis at equal intervals. The moment of appearance of such a region in current oscillolgrams corresponds to the current pulse. Thus, we can conclude that the image obtained corresponds to the EW flow produced by a single Tritchel pulse. A further increase in the voltage results in an increase in the pulse repetition rate.

Figure 14 shows the distribution of velocity level lines for a negative needle and a voltage of 11.3 kV (data were processed using the MatLab software) and also the current lines of the electric wind. One can see that the flows have a very short acceleration zone ($\sim$ 1 mm) lying under the needle, then the velocity continuously decreases in the longitudinal direction, and the current lines are mutually parallel. In the acceleration zone, the Coulomb force acts on the air and then the jet is decelerated by friction forces.

Unlike negative polarity, the CD cover for positive polarity has the surrounding shape, which does not change until the appearance of streamers. Therefore, here, such a variety of phenomena does not appear, Tritchel pulses are absent, and, beginning with the ignition threshold, the EW has a stationary nature. Note here that the width of a small EW jet for the positive corona is smaller than that for the negative corona (Fig. 14). In addition, negative ions produced by attached electrons do not enter the external region, which is filled with positive ions coming directly from the ionization region. Therefore, the density of positive ions is higher, and the high-density region with positive ions is more compact. As a result, the radius of an EW jet from the positive electrode is considerably smaller and approximately corresponds to the radius of the needle electrode end.

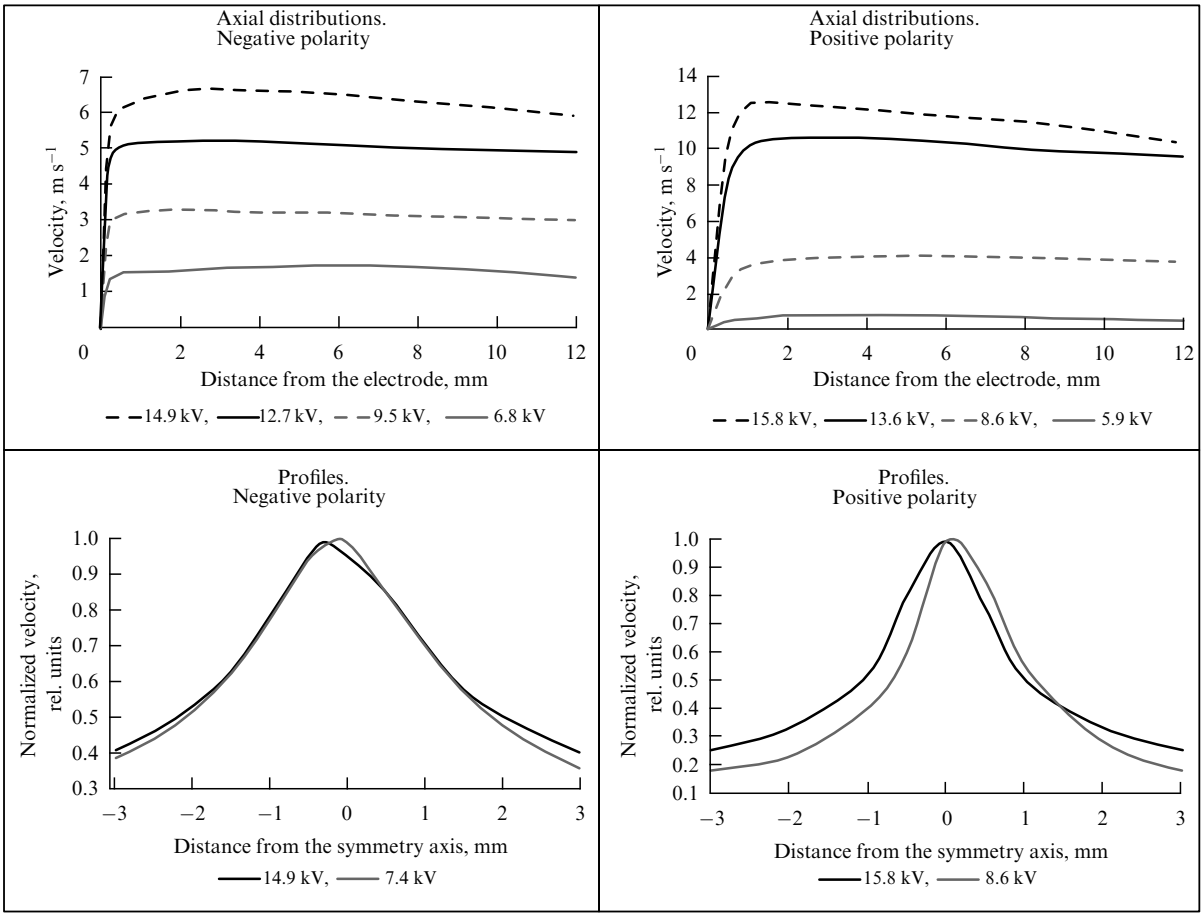

Figure 15. Axial distributions and air velocity profiles for negative and positive needle polarities.

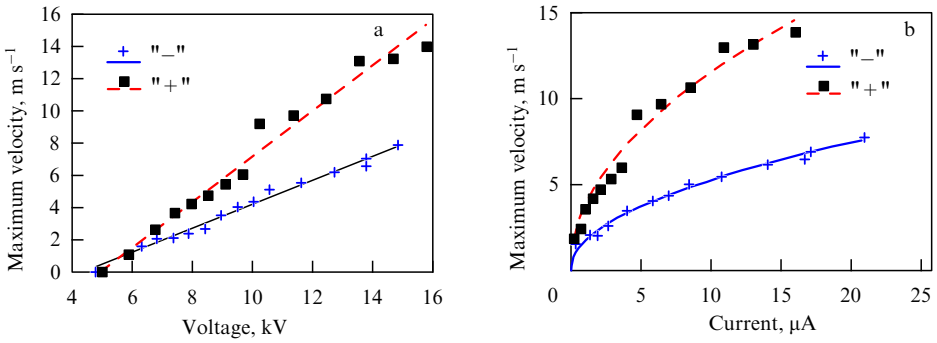

Figure 16. Dependences of the maximum velocity on the voltage (a) and current (b). Dashed curve — positive polarity, solid curve — negative polarity. Squares and crosses are experimental data.

Note also that the maximum velocity for the positive polarity is almost twice that for the negative polarity. Let us consider normalized velocity profiles at a distance of 5 mm from the needle end for various polarities and voltages (Fig. 15). We can find from these plots that the radius of the EW jet for the negative polarity is approximately 4 mm, while this radius for the positive polarity is ~ 2 mm. Thus, we confirmed the conclusion made above based on the qualitative analysis of contour plots.

Let us compare axial velocity distributions for positive and negative polarities (Fig. 15). It can be seen that the acceleration zones for both polarities approximately coincide, and the zone size is smaller than 1–2 mm, which corresponds to the characteristic size of the CD cover. Behind the acceleration zone, the velocity weakly decreases along the axis for the negative polarity. In the case of positive polarity, the velocity decreases more strongly at high voltages.

It is known from earlier studies that, above the CD threshold, the mean EW velocity (flow rate in the central jet) is proportional to the voltage [3]. This is confirmed by our investigations (Fig. 16).

It follows from Fig. 16 that the dependence of the maximum velocity [and, therefore, the mean velocity,

because the EW velocity profiles are similar for all voltages (Fig. 15)] on voltage is linear. Thus, the data obtained satisfy known empirical dependences.

Modern laser anemometry studies of the EW confirmed earlier results on the EW structure [3], while also giving some new results:

(1) In the region of threshold voltages in the pulsed negative corona regime, pulsed EW was observed consisting of individual charged mushroom-like regions moving in the interelectrode gap with velocities of about 30 cm s^{-1}.

(2) The EW flow in the stationary regime has a Gaussian velocity profile independent of the voltage, while the longitudinal velocity distribution has a zone structure consisting of a short acceleration zone and a long quasi-homogeneous flow zone.

(3) The EW jet radius is determined by the CD cover structure: for a negative polarity of the needle electrode, the jet radius is twice this radius for positive polarity.

(4) The dependence of the mean EW velocity (flow rate) on voltage is linear, while the dependence on current is a root type.

6. Simplified model of a corona discharge and electric wind

Computer EW simulations based on a complete system of equations involving ionization processes in the CD cover are possible (see Figs 6, 7) but extremely time-consuming. For this reason, simplified models are developed mainly based on the unipolar approximation: only the external zone of the discharge is considered, where charged particles of the same sign (corresponding to the polarity of the active electrode) are present and ionization is absent [43]. The CD cover in such models is described by the boundary condition. Two approaches are mainly used (a comprehensive list of studies on EW simulations indicating the type of boundary conditions used is presented in reviews [3, 43]).

The first approach, which is quite popular, is based on using the experimental volt-ampere characteristic (VAC). The flow density j_- of negative ions is specified as a function of the field strength E:

$$j_-(E) = C(E - E_0)\,.$$

Constants C and E_0 are selected to fit the experimental VAC with the theoretical one. The obvious disadvantage of this approach is that the VAC will change after any geometrical modification, and it will be necessary to measure it again in experiments and select the values of C and E_0.

The second approach uses the fact that the field strength on the active electrode surface is constant:

$$E = \text{const}\,.$$

As a constant, values close to the critical field strength (25 kV cm^{-1}) are used. For a cylindrical electrode, Pick's formula is used [44]. This condition in the general case is inapplicable for an entire high-voltage electrode and, therefore, it is necessary to separate on it a corona region, which is a problem.

In addition, analytic estimates are used for specific electrode shapes, especially for a cylindrical electrode [45]. There are also fundamentally different approaches. For example, in [46], the volume charge density is specified on the corona surface of the electrode. However, this quantity cannot be measured in experiments.

Thus, several widely used methods exist. However, each of them has significant disadvantages. In [47–49], the boundary condition is proposed in the original form of the relation for the growth rate of the flow density of charged particles from the CD cover:

$$\frac{\partial j_e(b,t)}{\partial t} = j_e(b,t)\,\frac{\gamma \exp(M) - 1}{\tau}\,, \tag{6.1}$$

$$\tau = \int_a^b \frac{dy'}{\mu_+ E(y')}\,, \tag{6.2}$$

$$M = \int_a^b \alpha\big(E(y')\big)\,dy'\,. \tag{6.3}$$

Here, integrals (6.2) and (6.3) are taken along the force line ab, and y' is a coordinate along this force line. There are plenty of force lines: b is a variable giving a point on the active electrode (it is clear that each such point corresponds to its own force line), and M is the number of ionization collisions on a force line of the electric field coming to the point b. Thus, M, as the density j_e of current entering air, can be considered a function defined on the active electrode surface. Relation (6.1) can be treated as an extension of the known condition of maintaining a self-sustained discharge [1] $\gamma \exp(M) - 1 = 0$ to the nonstationary case. Using some assumptions, we can derive it from system (1) in the drift-diffusion approximation [47].

In the model used here, the CD cover, whose structure is found in the drift-diffusion approximation (see Fig. 6), is reduced to Eqn (6.1) solved on the active electrode surface. Such a model can be used for calculating distributions of particle concentrations, velocity fields in the external CD region, and some integral characteristics. The focus structure is not considered in this model.

Note that the question of how correct this model is in the case of a multi-focus negative CD (Fig. 2b) remains open. Because the structure and properties of the focus in the simplified model are described approximately, there is no reason to assume that the location of focuses appearing in a system with the multi-focus structure will correspond to reality.

Consider a positive CD in a needle–plane electrode system. For this system, velocity fields were obtained by the PIV method for different voltages, and calculations were performed in the unipolar model with boundary condition (6.1)–(6.3) in the drift-diffusion approximation (4), (5). The results of simulations and experiments are compared in Fig. 17.

Distributions of the volume electric charge in the unipolar (simplified) and drift-diffusion (complete) models are compared in Fig. 17a. Near the needle end (at a distance of approximately up to 1 mm), the simplified model predicts a considerably higher volume charge density than does the complete model. However, already at distances of several millimeters, this discrepancy disappears.

This difference in the volume charge near the needle end leads to the difference in velocities at the center reaching 1.5 times (Fig. 17c). However, the same plot shows that the difference is observed in a very narrow region about 0.1 mm from the symmetry axis. In the rest of the region, the velocity profiles are in good agreement. This means that integral characteristics (such as the air flow rate, the pressure force

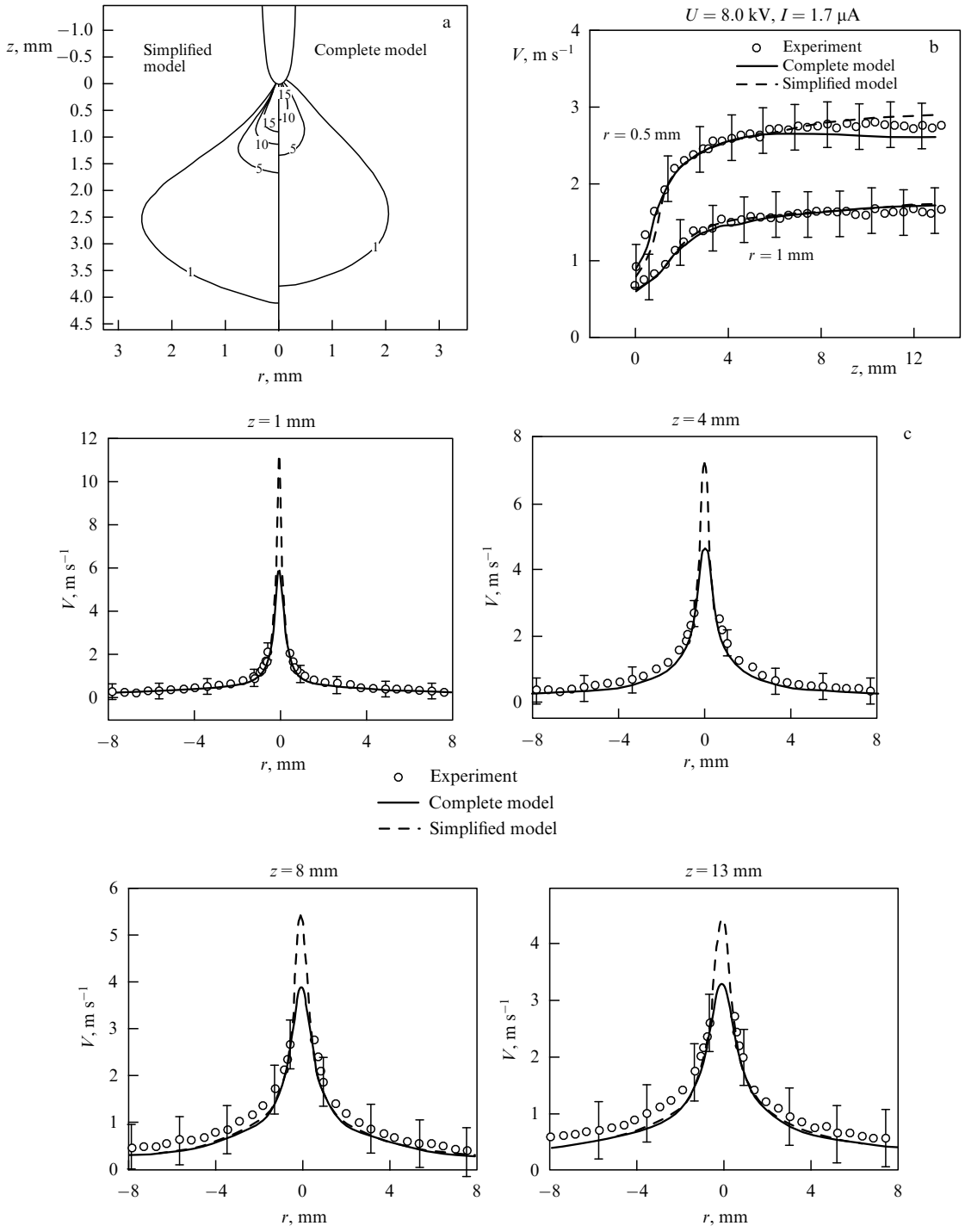

Figure 17. Comparison of the unipolar (simplified) and drift-diffusion (complete) CD models with experiments. Voltage $U = 8.0$ kV, current $I = 1.7$ μA. (a) Contour plots of the total volume charge (mC m^{-3}) for two models. (b) Velocity distribution along the z-axis. (c) Radial air velocity distributions at various distances z from the needle.

on the counter electrode) in the unipolar model will only slightly differ from those in the drift-diffusion model. The velocity values at the jet center have not been measured in experiments so far.

The velocity profiles measured in the jet are consistent with calculations (Fig. 17c) The jet gradually expands with distance from the needle end.

Experimental and model longitudinal velocity distributions constructed at distances of 0.5 and 1.0 mm from the symmetry axis of the model were quite similar (Fig. 17b). The acceleration region extends over 2–3 mm from the needle end. Note that this region approximately corresponds to the region of the main volume charge distribution (Fig. 17a) and the region of the volume force action. Next is located the region of slow viscous expansion of the jet, where the velocity is almost invariable.

A similar comparison made for the negative-polarity EW in the sphere–torus and needle–plane showed good agreement between calculations and experiments [48] (Fig. 18). Here, unipolar model calculations (6.1)–(6.3) were compared with

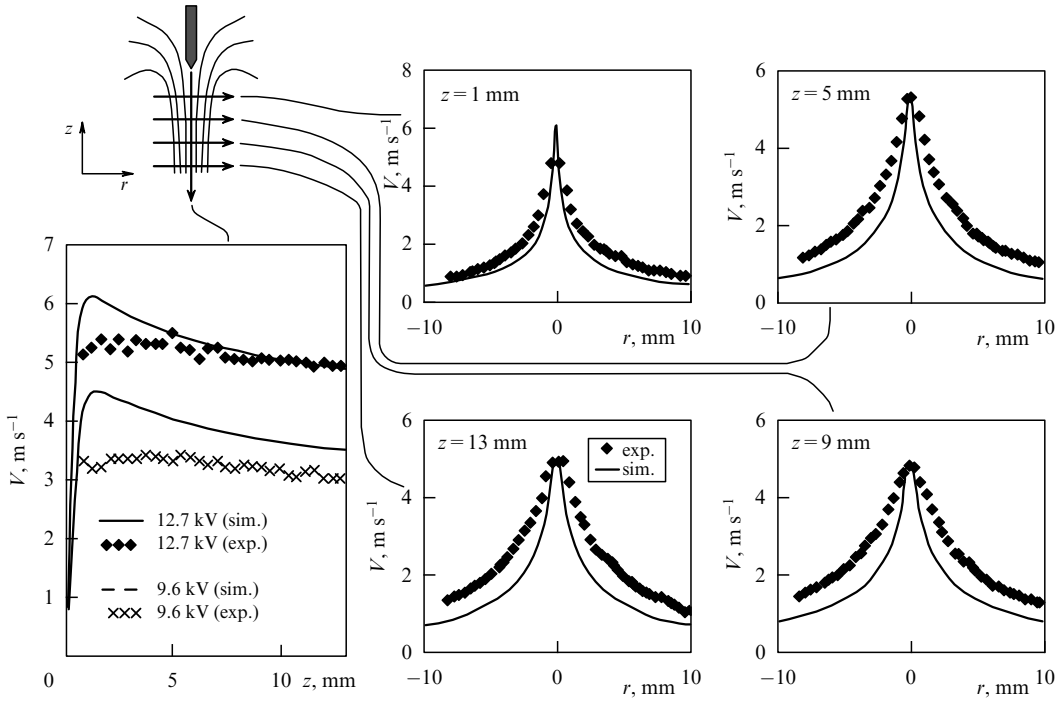

Figure 18. Transverse and axial velocity distributions in the needle–torus electrode system. Transverse distributions (dependences on the coordinate r) are constructed for the voltage 12.7 kV. Comparison of experiments (exp) with simulations (sim).

volt-ampere characteristics and velocity fields obtained by the PIV method. Figure 18 shows velocity distributions in the needle–plane electrode system. The flow structure resembles the positive polarity (cf. Fig. 17). Among differences, we point to a greater jet width (at a distance of 8–9 mm for the negative polarity, the jet radius at which the velocity is half the maximum value is about 4 mm, whereas for the positive polarity, this radius is about 1 mm) and a smaller acceleration region.

7. Conclusions

(i) Modern experimental CD studies have shown a strong dependence of the CD cover on the corona electrode polarity.

(ii) The structure of the negative CD cover is a focus type; the light region of the negative CD has a mushroom-like shape.

(iii) The structure of the positive CD cover has the surrounding shape: a thin luminous layer surrounding the electrode surface.

(iv) Computer CD simulations explained the dependence of the CD cover structure on the corona electrode polarity and revealed features of the ionization region.

(v) The ionization region of the negative CD has an egg-like shape and is located at some distance from the spherical electrode. The ionization zone of the positive CD has the shape of a thin layer surrounding the spherical electrode. The light region of the negative CD is considerably greater than the ionization region. For the positive CD, the size and shape of the ionization and light regions coincide.

(vi) The simplified EW model using the original boundary condition more accurately describes the EW structure than the earlier models constructed in the unipolar approximation.

References

1. Raizer Yu P *Gas Discharge Physics* (Berlin: Springer, 1997); Translated from Russian: *Fizika Gazovogo Razryada* (Dolgoprudnyi: Intellekt, 2009)
2. Vatazhin A B, Likhter V A, Ulybyshev K E *Fluid Dynamics* **47** 206 (2012); *Izv. Ross. Akad. Nauk Mekh. Zhidk. Gaza* (2) 78 (2012)
3. Vereshchagin I P *Koronnyi Razryad v Apparatakh Elektronno-Ionnoi Tekhnologii* (Corona Discharge in Electron–Ion Technology Devices) (Moscow: Energoatomizdat, 1985)
4. Fridman A, Chirokov A, Gutsol A *J. Phys. D* **38** (2) R1 (2005)
5. Pai D Z, Lacoste D A, Laux C O *J. Appl. Phys.* **107** 093303 (2010)
6. Akishev Yu et al. *Plasma Sources Sci. Technol.* **14** (2) S18 (2005)
7. Yang F et al., in *High Voltage Engineering. Proc. of the XIIIth Intern. Symp. on High Voltage Engineering, Delft, Netherlands, 25–29th August 2003* (Ed. J J Smit) (Rotterdam: Millpress, 2003) p. 155
8. Go D et al. *J. Appl. Phys.* **102** 053302 (2007)
9. Korchemkin I N, Stishkov Yu K, in *Abstracts of the 5th Intern. Conf. on Materials Science and Condensed Matter Physics and of Symposium "Electrical Methods of Materials Treatment" in Memoriam of Acad. Boris Lazarenko, Chisinau, Moldova, 2010*, p. 266
10. Chen I Y et al. *Int. J. Heat Mass Transfer* **57** 285 (2013)
11. Ong A O, Abramson A R, Tien N C *J. Heat Transfer* **136** 061703 (2014)
12. Siswanto W A, Ngui K *Australian J. Basic Appl. Sci.* **5** 1433 (2011)
13. Ianconescu R, Sohar D, Mudrik M *J. Electrostat.* **69** 512 (2011)
14. Léger L et al. *J. Electrostat.* **51–52** 300 (2001)
15. Léger L, Moreau E, Touchard G *J. Electrostat.* **64** 215 (2006)
16. El-Khabiry S, Colver G M *Phys. Fluids* **9** 587 (1997)
17. Colver G M, El-Khabiry S *IEEE Trans. Industry Appl.* **35** 387 (1999)
18. Vilela Mendes R, Dente J A *J. Fluids Eng.* **120** 626 (1998)
19. Zhao L, Adamiak K *J. Electrostat.* **63** 337 (2005)
20. Takeuchi N, Takubo K, in *Proc. of the Intern. Symp. on Electrohydrodynamics, ISEHD 2014, Okinawa, Japan, June 2014*
21. Mista W, Kacprzyk R *Catalysis Today* **137** 345 (2008)
22. Lai F C, Sharma R K *J. Electrostat.* **63** 223 (2005)
23. Boeuf J P, Pitchford L C *J. Appl. Phys.* **97** 103307 (2005)
24. Novák I, Pollák V, Chodák I *Plasma Process. Polymers* **3** 355 (2006)
25. Kim W et al. *IEEE Trans. Plasma Sci.* **34** 2545 (2006)
26. Lukes P et al. *J. Phys. D* **38** 409 (2005)

27. Malik M A, Ghaffar A, Malik S A *Plasma Sources Sci. Technol.* **10** 82 (2001)
28. Grabowski L R et al. *Plasma Chem. Plasma Process.* **26** 3 (2006)
29. Nagato K et al. *Int. J. Mass Spectrom.* **248** 142 (2006)
30. Dordizadeh P, Adamiak K, Peter Castle G S *J. Phys. D* **48** 415203 (2015)
31. Kasdi A *J. Electrostat.* **81** 1 (2016)
32. Dastoori K et al. *J. Electrostat.* **71** 351 (2013)
33. Shemshadi A, Niayesh K, Akbari A *Phys. Plasmas* **19** 073506 (2012)
34. Samusenko A V, Stishkov Yu K *Elektofizicheskie Protsessy v Gazakh pri Vozdeistvii Sil'nykh Elektricheskikh Polei* (Electrophysical Processes in Gases under Exposed to Strong Electric Fields) (St. Petersburg: VVM, 2011)
35. Zubkov T N, Samusenko A V, Stishkov Yu K *Surf. Eng. Appl. Electrochem.* **49** 474 (2013)
36. Samusenko A V, Safronova Yu F, Stishkov Yu K *Elekton. Obrabotka Mater.* **52** (5) 43 (2016)
37. Luque A et al. *Appl. Phys. Lett.* **90** 081501 (2007)
38. Stishkov Yu K, Samusenko A V *Surf. Eng. Appl. Electrochem.* **44** 271 (2008)
39. Vinaikin M Yu, Zuev D V, Stishkov Yu K, in *IX Mezhdunar. Nauchnaya Konf. ''Sovremennye Problemy Elektrofiziki i Elektogidrodinamiki Zhidkostei'', Sankt Peterburg, 22–26 Iyunya 2009 Goda. Sbornik Dokladov* (IX Intern. Sci. Conf. "Modern Problems of Electrophysics and Electrohydrodynamics of Liquids", St. Petersburg, 22–26 June, 2009. Proc.) (St. Petersburg: Solo, 2009) p. 217
40. Stishkov Yu, Samusenko A, Vinaykin M, Zuev D, in *Proc. of Intern. Symp. on Electrohydrodynamics, Malaysia, 2009*
41. Hamdi M et al. *Exp. Fluids* **55** 1702 (2014)
42. Kriegseis J et al., in *Proc. of the 50th AIAA Aerospace Sciences Meeting Including the New Horizons Forum and Aerospace Exposition, Nashville, Tennessee, 09–12 January 2012* (Reston, Va.: AIAA, 2012) p. AIAA0406
43. Adamiak K *J. Electrostat.* **71** 673 (2013)
44. Kaiser S, Fahlenkamp H, in *Proc. of the Intern. Symp. on Electrohydrodynamics, 23–26 September 2012, Gdańsk, Poland*, p. 101
45. Talaie M R, Taheri M, Fathikaljahi J *J. Electrostat.* **53** 221 (2001)
46. Nouri H, Zebboudj Y *Eur. Phys. J. Appl. Phys.* **49** 11001 (2010)
47. Samusenko A, Stishkov Yu, Zhidkova P *Int. J. Plasma Environment. Sci. Technol.* **9(1)** 24 (2015)
48. Ashikhmin I A, Samusenko A V, Stishkov Yu K, Yakovlev V V *Tech. Phys.* **60** 1637 (2015); *Zh. Tekh. Fiz.* **60** (11) 65 (2015)
49. Ashikhmin I, Stishkov Yu K, Yakovlev V *Int. J. Plasma Environment. Sci. Technol.* **9** 13 (2015)